Control of silicon nanoparticle size embedded in silicon oxynitride dielectric matrix

F. Ehrhardt, G. Ferblantier, D. Muller, C. Ulhaq-Bouillet, H. Rinnert, and A. Slaoui

Citation: Journal of Applied Physics **114**, 033528 (2013); doi: 10.1063/1.4816042
View online: https://doi.org/10.1063/1.4816042
View Table of Contents: http://aip.scitation.org/toc/jap/114/3
Published by the American Institute of Physics

Control of silicon nanoparticle size embedded in silicon oxynitride dielectric matrix

F. Ehrhardt,[1,a)] G. Ferblantier,[1] D. Muller,[1] C. Ulhaq-Bouillet,[2] H. Rinnert,[3] and A. Slaoui[1]
[1]*ICube, Strasbourg University-CNRS, 23 rue du Loess BP20, 67037 Strasbourg Cedex 2, France*
[2]*IPCMS, Strasbourg University-CNRS, 23 rue du Loess BP43, 67034 Strasbourg Cedex 2, France*
[3]*IJL, CNRS, Campus Victor Grignard BP 70239, 54506 Vandoeuvre-les-Nancy Cedex, France*

(Received 15 March 2013; accepted 2 July 2013; published online 19 July 2013)

In this study, silicon rich silicon oxynitride layers containing more than 15% nitrogen were deposited by electron cyclotron resonance assisted plasma enhanced vapor deposition in order to form silicon nanoparticles after a high temperature thermal annealing. The effect of the flows of the precursor gases on the composition and the structural properties of the layers was assessed by Rutherford backscattering spectroscopy, elastic recoil detection analysis, and infrared spectroscopic measurements. The morphological and crystallinity properties were investigated by energy filtered transmission electron microscopy and Raman spectroscopy. We show that the excess of silicon in the silicon oxynitride layer controls the silicon nanoparticles size. On the other hand, the crystalline fraction of particles is found to be strongly correlated to the nanoparticle size. Finally, the photoluminescence measurements show that it is also possible to tune the photoluminescence peak position between 400 and 800 nm and its intensity by changing the silicon excess in the silicon rich silicon oxynitride matrix. © *2013 AIP Publishing LLC*. [http://dx.doi.org/10.1063/1.4816042]

I. INTRODUCTION

Silicon nanocrystals (Si-ncs) have received a great interest in recent decades since they can be very useful in many applications such as for data storage,[1] lasers,[2] or photovoltaics.[3] These silicon nanocrystals are usually embedded in a dielectric matrix, which are often obtained upon high temperature annealing of silicon rich silicon oxide (SRSO)[4] or silicon rich silicon nitride (SRSN).[5] SRSO layers were thoroughly produced by Plasma Enhanced Chemical Vapor Deposition (PECVD) using SiH_4 and O_2 or N_2O[6] and resulted in Si-nps in SiO_2 matrix. On the other hand, Si-nps in Si_3N_4 matrix were obtained from SRSN layers by mixing SiH_4 and NH_3. The size of the nanoparticles is controlled by the excess of silicon present in the Si rich layer.[6] Another way to control the Si-ncs size is the use of superlattice in order to constrain the size of the nanoparticles within the size of the silicon rich layer.[7] From the application point of view, the final matrix surrounding the nanoparticles provides advantages and drawbacks depending on the desired device. For instance, LED devices based on nanocrystals in silicon oxide (SRSO) showed a better electroluminescence but exhibited a higher turn on voltage and current.[8] For photovoltaic devices using the quantum size effects provided by the silicon nanoparticles, the SiN matrix is more favorable because of a lower energy offset, and therefore, a better charges transport is expected.

Among alternatives as a host dielectric matrix, silicon oxynitride (SiO_xN_y) may be a good material since its electronic and optical properties can be tuned from SiO_2 to Si_3N_4 to match the device requirements. PECVD with silane (SiH_4) and nitrogen protoxide (N_2O)[9,10] is also used to produce silicon rich silicon oxynitride (SRSON). Most of the reported data[6–11] on Si-nps from SRSON layers exhibit a dielectric matrix surrounding the nanoparticles with a maximum of 15% nitrogen, which means close to a SiO_2 matrix. By changing the deposition conditions, it is possible to incorporate more nitrogen in the layers.[12,13]

We have previously presented the possibility to fabricate silicon nanocrystals in a silicon oxynitride layer matrix using a fixed flow of silane (SiH_4) and nitrogen protoxide (N_2O) of 20 and 10 sccm, respectively.[14] In this work, we report on the tuning of the nanoparticles size and distribution by varying the amount of incorporated nitrogen in the SRSON layers. We demonstrate that the change in gas flows results in SRSON films with different structural and optical properties. We show that less silicon excess is needed in the SRSON layers as compared to SRSN to reach a similar nanoparticle size. We also show a strong correlation between the fraction of crystalline silicon (c-Si) nanoparticles and the amount of silicon atoms in excess present in the SiON matrix.

II. EXPERIMENTAL DETAILS

Silicon rich silicon oxynitride layers were deposited on p-type (100) silicon wafers and quartz substrates using an Electron Cyclotron Resonance Assisted Plasma Enhanced Vapor Deposition (ECR-PECVD) system. The deposition process is divided in 3 steps. First, the substrate is heated up to 400 °C in 5 min under flows of nitrogen protoxide and silane and then the plasma is turned on to start film deposition. The deposition time was fixed to 20 min for all samples. The microwave (MW) power source was fixed at 500 W, and the radiofrequency (RF) power source was adjusted automatically. Finally, the gas flows are stopped, and the substrate was cooled down to room temperature before downloading

[a)]Author to whom correspondence should be addressed. Electronic mail: Fabien.ehrhardt@etu.unistra.fr

the samples. The flow of the N_2O gas was fixed at 10 sccm while that of SiH_4 was varied from 10 to 22 sccm. We defined a parameter R as the ratio between the N_2O and the SiH_4 gas flows ($R = N_2O/SiH_4$). For our experiments, R was therefore varied from 0.45 to 1. This parameter can be considered as the key to tune the structural and optical properties of the deposited SRSON layers. In order to obtain the phase separation, the SRSON layers were annealed at 1100 °C for 1 h in Argon atmosphere. The final thickness is ranging between 300 and 400 nm. Rutherford Backscattering Spectroscopy (RBS) and Elastic Recoil Detection Analysis (ERDA) methods were employed to extract the chemical composition of the SRSON layers before and after annealing. Fourier Transform Infrared (FTIR) spectra were used to determine the chemical bonding in the as deposited and annealed layers. Photoluminescence (PL) spectra were recorded at room temperature using a 355 nm excitation wavelength of an Nd:YVO_4 laser. The emitted light was detected by a spectrometer coupled with a CCD linear image sensor. The response of the detection system was precisely calibrated with a tungsten lamp calibration source. Finally, High Resolution Transmission Electron Microscopy (HR-TEM) and Energy Filtered (EF)-TEM measurements on cross sectional specimens were performed with a JEOL2100F microscope operating at 200 kV, equipped with a corrector for spherical aberration and the TRIDIEM Gatan imaging filter. The cross sectional specimens were prepared by the tripod method and finished by a gentle ion milling step. The EF-TEM images were formed by the electrons which were selected with a slit placed in the energy dispersive plane of the spectrometer at the plasmon energy of the silicon at 17 eV with a width of ±2 eV.[15] In order to avoid multiple interaction, the analyses were proceeded in a very thin region ($t/\lambda < 0.2$ with t is the sample thickness and λ the mean free path of the electron.) Finally, Raman spectra were recorded on SRSON samples deposited on quartz substrates excited with a 532 nm laser to quantify the crystalline fraction of the silicon nanoparticles.

III. RESULTS AND DISCUSSION

A. Composition of the as deposited SRSON layers

Figure 1 plots the amount of silicon, oxygen, nitrogen, and hydrogen present in the as-deposited SRSON samples as a function of the gas ratio R. These atomic contents in the SRSON layers were determined by RBS and ERDA. It is found that silicon and hydrogen contents within the layers gradually decrease when increasing the gas ratio R (decrease of the SiH_4 flow) and tend to saturate for $R > 0.7$ reaching values of about 33% Si and 5–7% H. Concerning oxygen atoms, its content increases from 17% to 33% with increasing R. Such behavior is explained as the result of the presence of more N_2O in the gas mixture which is bringing oxygen during deposition. On the other hand, the atomic content of nitrogen in the layer behaves irregularly as compared to the other species: it increases for R between 0.45 and 0.67, goes through an optimum of about 36% at $R \sim 0.7$ and then decreases. This trend can be attributed to the change in gas composition during the layer deposition. Increasing R gradually means that more N_2O gas is injected in the reactor as compared to SiH_4 leading to an increased of nitrogen content in the layer.

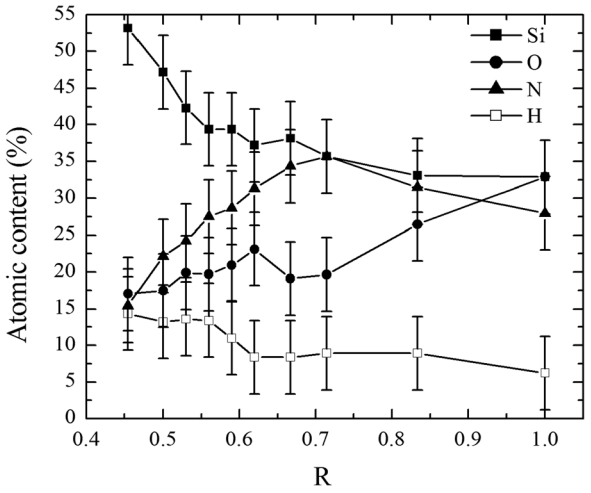

FIG. 1. Composition of the as deposited silicon oxynitride as determined by RBS and ERDA measurement for different gas ratio.

Increasing further R means that less silicon is available to be linked to more nitrogen and oxygen species present in the chamber. Since the bond energy of Si-O (799.6 kJ/mol) is higher than that of Si-N (470 kJ/mol),[16] silicon will more likely link to oxygen than to nitrogen. Less nitrogen is therefore present in the deposited film which might turn to a SiO_2 film for very high R values ($R > 1$). The data of Figure 1 show clearly that it is possible to control the amount of silicon and nitrogen in the SRSON layer.

To get more insights, FTIR analyses were recorded on as-deposited SRSON samples to study the chemical bonds. In particular, the FTIR technique was used to identify the presence of Si-O and Si-N bonds in the layers. Figure 2 plots FTIR spectra for $R = 0.45$, $R = 0.59$, and $R = 1$. All spectra exhibit a large band between 700 and 1300 cm^{-1}. This wide band is the result of contributions from many atomic bonds in the SRSON layer. The Si-O bending and stretching modes, respectively, absorb around 800 and 1050 cm^{-1}.[17,18]

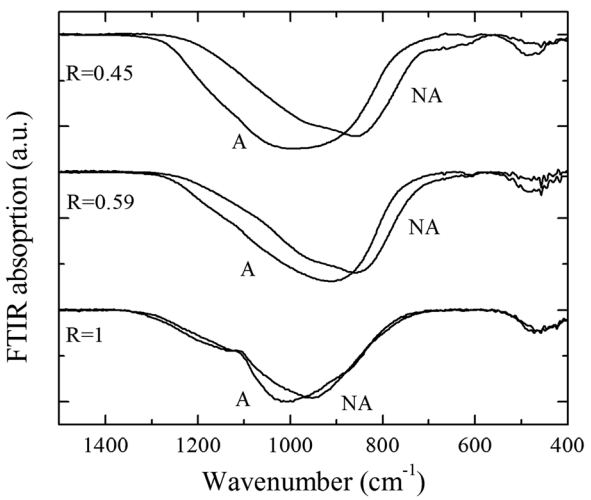

FIG. 2. FTIR spectra of different layers before annealing (NA) and after annealing (A).

The Si-N stretching mode is known to absorb at around 850 cm^{-1}.[17] The shoulder located at the 1100–1250 cm^{-1} can be attributed to the out of phase oxygen stretching mode.[18,19] For the as-deposited samples, the different hydrogen chemical bonds were also taken into account. Thus, the FTIR spectra show a Si-H bending mode at 650 cm^{-1} and the N-H rocking mode at 1150 cm^{-1}.[5]

We have found that for a gas ratio of 0.45 and 0.59 the absorption band maximum is relatively constant at 860 cm^{-1}; then, the whole band position shifts to reach 952 cm^{-1} for R = 1. The shift to the high wavenumbers for high R values can be explained as due to an increase of Si-O bonds and a decrease of Si-N bonds. This is in strong agreement with the RBS data shown above.

The FTIR analysis was also used to detect hydrogen bonds in the deposited layers. The N-H stretching mode and the Si-H stretching mode are found (not shown here) to absorb around 3400 cm^{-1} and 2000 cm^{-1},[17] respectively. However no O-H bond were detected around 3600 cm^{-1} range like in the work of Denisse *et al.*[10] Therefore, we consider that only Si-H and N-H bonds for hydrogen are present in our SRSON layers. According to Lanford *et al.*,[20] the total hydrogen content in a SiNx:H is proportional to the absorption area of the Si-H + 1.4 times the area of the N-H band. Using this method, the H bonds concentration was calculated for the different deposited layers. Figure 3 plots the calculated atomic hydrogen bonds with silicon and nitrogen for the as-deposited SRSON layers versus the gas ratio R. For R < 0.6, hydrogen has more bonds to silicon than to nitrogen while for high gas ratio hydrogen is more preferentially bonded to nitrogen.

B. Composition of the annealed SiO_xN_y layers

After thermal annealing of the as-deposited SRSON layers at 1100 °C, no hydrogen atoms can be detected anymore by ERDA as a consequence of its exo-diffusion from the layer.

The hydrogen exo-diffusion from the SRSON:H upon annealing can be described by the following reactions:

$$SiH + NH \rightarrow SiN + H_2 \uparrow, \quad (1)$$

$$SiH + SiH \rightarrow SiSi + H_2 \uparrow . \quad (2)$$

It is clear from the Eqs. (1) and (2) that the breaking of a Si-H bond is potentially a source for silicon atoms in excess while an N-H bond will consume a silicon bond to form Si-N. For high R values, the number of Si-H bond is lower than for N-H before annealing. Some N-H bonds may react together to form nitrogen molecules that leave the film. Thus, some nitrogen loss is expected after thermal annealing.

Figure 4 plots the atomic content of silicon, nitrogen, and oxygen atoms in the annealed SRSON layer as determined by RBS analysis. The general trend is similar to what was observed before annealing (Figure 1). The oxygen content is almost constant over a large range of R values and suddenly increases for R > 0.7. The nitrogen content is found to increase from 20 to 35% in the layer, well above the 15% reported elsewhere. The decrease of N content for a gas ratio higher than 0.7 can partially be due to the loss of nitrogen atoms during annealing.

From the molecular structure point of view, the possible bonds in the annealed layers are Si-Si, Si-O, Si-N, O-N, O-O, and N-N. However, O-O, N-N, and O-N have a high binding energy and will be neglected afterwards.[16] Therefore, only left are Si-Si, Si-O, and Si-N bonds. The silicon excess (Si_{excess}), which is the silicon available for the formation of Si nanoparticles in the host matrix, can then easily be defined. Si_{excess} is considered in SiON as a quarter of the number of Si-Si bonds. By using the valence of each atom, Si_{excess} can be expressed as[10]

$$Si_{excess} = \frac{1}{4}(4 \times Si - 2 \times O - 3 \times N). \quad (3)$$

Figure 4 plots also the atomic silicon excess Si_{excess} (stars) versus the gas ratio after thermal treatment of the SRSON layers. For gas ratio from 0.45 to 0.65, the silicon excess decreases from 35% to about 4%, and it seems to be strongly correlated to the nitrogen content in the layer. For high gas

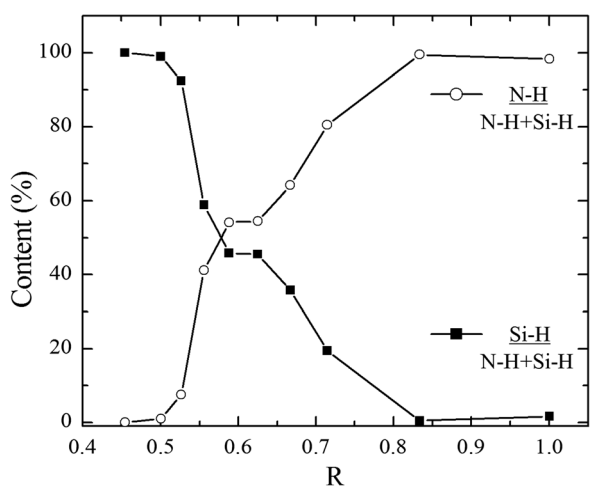

FIG. 3. Atomic Hydrogen bonds with silicon and nitrogen for as-deposited SRSON:H layers versus the gas ratio R.

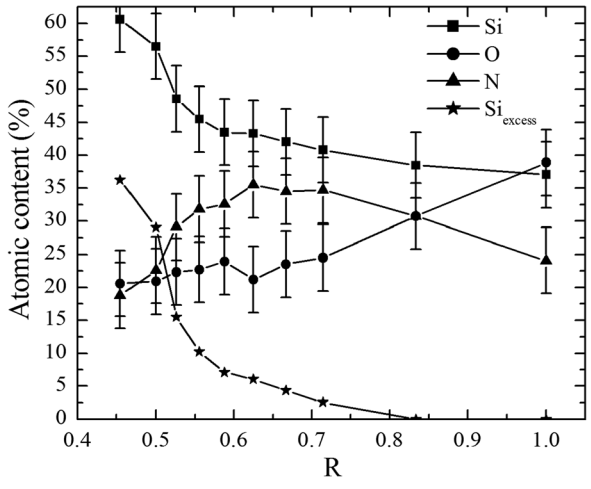

FIG. 4. Atomic composition in the annealed silicon oxynitride layers at 1100 °C for 60 min as determined by RBS measurements for different gas ratio.

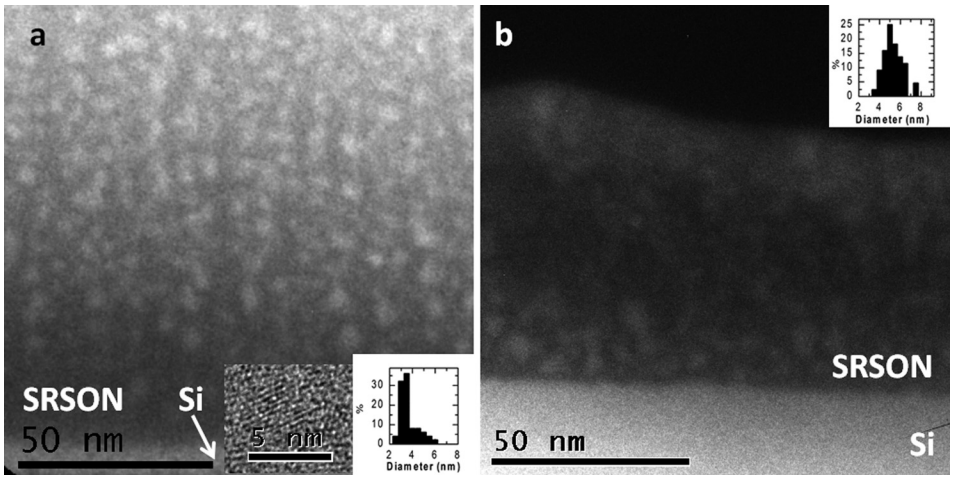

FIG. 5. EFTEM image for SRSON films containing an excess of silicon of (a) 7% and (b) 15%.

ratio ($R \geq 0.7$), the excess of silicon is very small ($\leq 2\%$). For very high gas ratio, the SRSON tends to a SiO_2 matrix. These results show that the excess of silicon can be easily tuned in an annealed SRSON layer by controlling the gas ratio during the plasma deposition process, which in turns controls the amount of nitrogen in the layer.

To complete the study on the composition of the annealed SRSON films, FTIR analysis were carried out. The measured spectra are also reported in Figure 2 for different R values. For a fixed R, the spectrum of the annealed sample is different from that recorded for the nonannealed one. The peak position and the shape of the large band are varying versus the R value. For $R = 0.45$, the wide band centered at about $1000\,cm^{-1}$ indicated the formation of a SiON matrix with somehow equal contribution of Si-O and Si-N bonds. At $R = 0.59$, the peak position is closer to the Si-N bond position, which means that the annealed film is N-rich. In contrast, the peak position for the annealed sample with $R = 1$ is strongly shifted towards the Si-O bond position which indicate the formation of an oxygen rich film. Such observations are consistent of the RBS data giving the atomic composition in the annealed layers (Figure 4).

Thus, the difference in FTIR spectra recorded before and after annealing is probably due to the reorganization of the matrix and a relaxation of the bonds. In essence, a stoichiometric silicon oxide is only composed of Si-O while a silicon nitride is composed of Si-N bonds. However, SiO_x and SiN_x deposited layers are not thermally stable. A phase separation into Si nanoparticles and stoichiometric SiO_2 or Si_3N_4 after annealing at high temperature of deposited SiO_x or SiN_x films, respectively, is highly expected. The as deposited SRSON layers do not present a stable phase either. Therefore, the SRSON layer can also decompose into two separate phases, namely, a Si phase and a SiON matrix. The Si phase allows the growth of silicon nanoparticles.

C. Identification of the silicon nanoparticles

EFTEM analysis was carried out exclusively on annealed SRSON layers to assess the formation of silicon nanoparticles in the SiON matrix. EFTEM characterization carried out for samples with 4 and 6% excess of silicon in the layer did not show any silicon particles. If they exist, their size should be smaller than the detection limit of EFTEM which is ~ 1.5 nm.[21] On the other hand, EFTEM images for samples with a Si_{excess} of 7% and 15% are shown in Figure 5. Silicon nanoparticles appear in white within a dark SiON matrix. From these images, the particle average size and its distribution can be estimated. The nanoparticles are considered to be sphere-shape with a defined diameter. The extracted values are reported in Figure 6. The diameter of the particles is found to decrease from 6.8 to 3.2 nm when R increases (nitrogen content increases). The decrease of the particles size is easily understandable with the reduction of the silicon excess amount in the SRSON layer. As the silicon excess is decreasing, there are less silicon atoms available for the formation of silicon nanoparticles. Furthermore, with increasing R, the SiON matrix contains more nitrogen, which slow down the diffusion of silicon atoms,[17] resulting in smaller nanoparticles.

The Si nanoparticles shown in Figure 5 seem to be organized in a vertically ordered shape. It has already been shown that for high excess of silicon, the nanoparticles form nanocolumns.[14,21] Nanoparticles become laterally connected and form elongated particles due to a spinodal decomposition.[22]

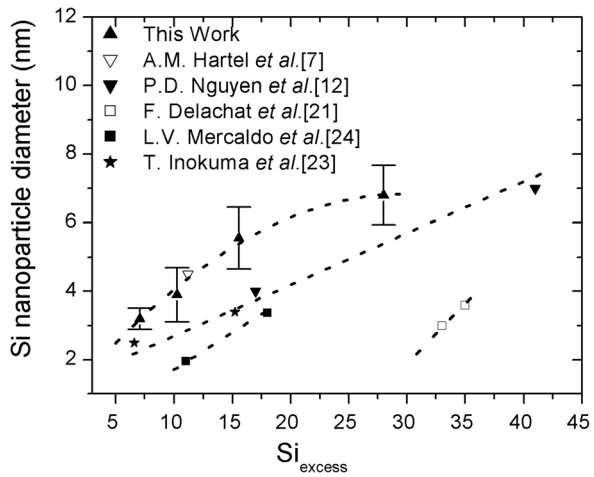

FIG. 6. Average diameter extracted from EFTEM images of high temperature annealed SRSON layers as a function of silicon excess that it contain. The Si excess was determined from RBS analysis. Some data from the literature are also shown for silicon nps within SiO2,[23] SiON,[7,12] and SiN[21,24] matrix.

Before forming the nanocolumns, the nanoparticles may align like in Figure 5(a).

In Figure 6 are drawn some results from the literature for SiO (stars), SiN (square), and SiON matrix (triangle.) The reported data are for silicon nanoparticles obtained at a similar thermal budget, namely 1100 °C. It is found that for a given silicon excess, we obtain larger nanoparticles. This difference can be attributed at first glance to the difference in the dielectric matrix. Other samples prepared in our lab with a higher oxygen proportion in the dielectric matrix shows a smaller size than those present in this paper at an equivalent excess of silicon.

The silicon nanocrystals average size is found to be larger within silicon oxynitride SiON than within silicon oxide SiO_2 or silicon nitride SiN for a comparable silicon excess value. During the annealing process, the silicon atoms in excess in the matrix nucleate to form small nanocrystal. When all the silicon in excess is consumed, the growth of the nanocrystals is governed by the Ostwald ripening, known as Lifshitz-Slyozov-Wagner (LSW) theory.[25,26] This result was recently confirmed by Roussel *et al.*[27] using the atomic probe tomography tool that permits to measure the silicon concentration in the silicon oxide for different annealing time. In the LSW theory, the smaller silicon nanoparticles decrease in size, while the silicon atoms in excess move towards the larger nanoparticles. The evolution of the average radius r of the silicon nanoparticle during this process is modeled by the Eq. (4).[25,26] In this formula, D and C are, respectively, the diffusion coefficient and the solubility limit of silicon in the dielectric matrix, t is the time, r_0 and t_0 are respectively the initial radius and time, γ is the interfacial energy, υ is the atomic volume of the solute, k the Boltzmann constant and T is the temperature.

$$r^3 - {r_0}^3 = \frac{8}{9} DC \frac{\gamma \upsilon}{kT} (t - t_0). \quad (4)$$

Equation (4) shows that the radius r is strongly dependent on the parameter DC. The more important is this parameter the larger is the size of the silicon nanocrystal as the flow of atoms is high. The diffusivity D of silicon in silicon oxide is found to vary depending on the deposition and characterization methods used. This was explained by Roussel *et al.*[27] The diffusivity coefficient of silicon in silicon oxyde depends on the supersaturation of silicon. Nevertheless in the LSW theory it is assumed to have a very small supersaturation. An average value of 5.7×10^{-18} cm^2/s can be considered.[28] The diffusion of silicon in silicon nitride is almost two order of magnitude lower, as it is about 2.7×10^{-20} cm^2/s.[29] On the other hand, the solubility C of silicon in silicon oxide is smaller than in silicon nitride. Considering our structure which is silicon in silicon oxynitride, the corresponding D and C data should have intermediate values and the resulting DC product is expected to go through a maximum value. Figure 6 shows indeed that the obtained nanoparticles diameters seem to be much larger for SiON matrix than for SiO_2 or SiN ones.

It should be noticed that the LSW model was developed for highly diluted systems. A modified LSW was proposed[30] to take into account the case of high volume fraction in the matrix, which means large silicon excess in our case. The new model[30] predict an increase of the size of the nanoparticle with the excess of silicon which is in good agreement with our results reported in Figure 6. As for the silicon nanoparticles density, it changes also versus the deposition parameters such as the thermal budget[27] and gas compostion.[14]

Presence of Si nanoparticles in the SiON matrix was witnessed by EFTEM measurements, but it does not give an insight on their degree of crystallinity nor on their crystalline orientation. For more information on the crystalline properties of the Si nanoparticles, HRTEM measurements were performed. Thus, a large fraction of silicon nanocrystals were observed for layers deposited at low gas ratio ($Si_{excess} \geq 10\%$) while no Si crystals were visible for the 4% Si_{excess} sample. It should be noticed however that the HRTEM analysis allows only the observation of oriented nanocrystals towards the electronic beam. Therefore, a complementary Raman study is required to assess the crystallinity of the particles and the fraction of crystalline part as compared to the amorphous ones.

Raman spectra recorded on annealed SRSON samples on quartz and containing different excess of silicon are shown in Figure 7. The wide emission band is due to different contributions. The contribution at 300, 380, and 480 cm^{-1} corresponds, respectively, to the LA, LO, and TO modes in the amorphous silicon (a-Si).[31] The TO signature of c-Si is a peak at around 510-520 cm^{-1} depending on the nanocrystal size.[31] A deconvolution with a Lorentzian peak for the c-Si and four Gaussians corresponding to the 3 a-Si peaks and a peak at 500 cm^{-1} was applied. The peak at 500 cm^{-1} is due to Si objects with a more ordered structure than amorphous silicon but not as ordered as crystalline silicon. This Si objects can be an intermediate phase of silicon,[32] grain boundaries[33] and/or very small nanocrystal grains of about 1 nm in size.[34]

For the sample containing a Si excess of 4%, the Raman spectrum is composed of the contributions at around 300,

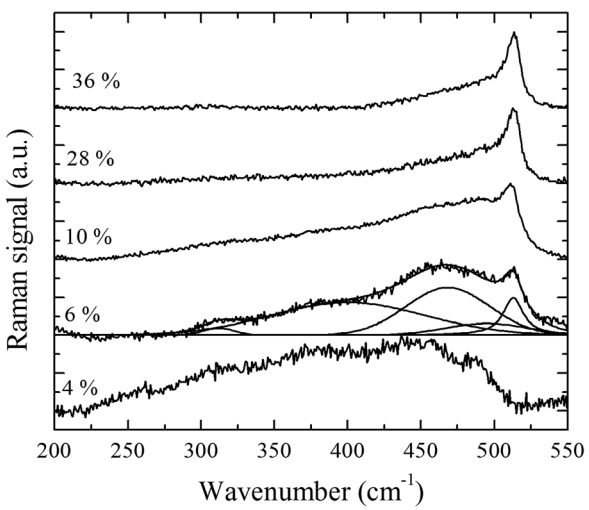

FIG. 7. Raman spectra recorded for high temperature annealed SRSON layers containing different excess of silicon. The Si excess was determined from RBS analysis.

380, and 480 cm^{-1}, which are the signatures of the amorphous silicon phase in the matrix plus that of the contribution of the substrate. No Si crystalline contribution is detected. Thus, the Raman signal confirms the presence of silicon in excess, but there is no proof that the silicon atoms have generated Si nanoparticles. The substrate contribution was also measured on samples deposited with a smaller Si_{excess} but there was no trace of amorphous silicon contribution.

For the sample containing a Si excess of 6%, the Raman spectrum of this sample shows a crystalline contribution while its EFTEM image did not reveal Si nanoparticles embedded in the SiON layer. The Raman peak intensity at 513 cm^{-1} is obviously weak, but the position tends to indicate the presence of Si nanocrystals. This contradiction may be attributed to the limited EFTEM resolution, which is typically around 1.5-2 nm. Thus, the SRSON sample with 6% Si_{excess} might contain nanoparticles having a diameter size smaller than 1.5 nm.

For samples with higher Si excess (>10%) in the SiON layer, the contribution of the TO mode for crystalline silicon is more pronounced as compared to the others. From the Raman data, the crystalline fraction was quantified using $X_c = I_c/(I_c + yI_a)$ where I_c and I_a are the integrated scattered intensity of the TO mode of c-Si and a-Si, respectively, and $y(D) = 0.1 + \exp(-D/25)$ with D the crystallite diameter in nm.[35] For our SRSON samples, we choose y = 0.88 according to Sui *et al.* work.[34] The X_c data are given in Figure 8 versus Si_{excess} in the matrix. As the excess of silicon increases (nitrogen content increases), the crystalline fraction increases. This is in agreement with Hernandez *et al.*[36] As expected, large silicon nanoparticles crystallize more easily than the small ones for temperatures up to 1100 °C. The proportion of Si objects is also calculated through the equation $X_{ip} = I_{ip}/(I_{ip} + I_c + yI_a)$,[33] where I_{ip} is the integrated scattered intensity of the intermediate phase. These data are also plotted in Figure 8. This fraction seems to increase when increasing Si_{excess}. However, the increase of X_{ip} is much more moderate than that of X_c, which indicates that the crystallinity of the nanoparticles is strongly correlated to the amount of silicon atoms in excess within the SiON matrix. In Yue *et al.* work reporting on crystallization of amorphous silicon, they have found that the X_{ip} phase fraction decreases when the crystalline fraction increases. Based on the results of Figure 6 showing that the high Si_{excess} generate larger nanoparticles, we speculate that by increasing the size of the nanoparticle, the nanocrystals coalesce and form multicrystalline nanoparticles. This can explain the increase of X_{ip} with Si_{excess}.

D. Photoluminescence of the SRSON layers

Photoluminescence spectra for annealed SRSON samples are shown in Figure 9. The excitation source is a laser emitting at 355 nm. It is found that the photoluminescence signal changes strongly with the variation of the Si_{excess} (nitrogen content): the PL peak position shifts and the intensity vary. The exact causes of the luminescence of the annealed SiO_xN_y layers are presently still under debate as contribution of defects are often hiding other effects. Thus, the observed overall PL signal can be attributed to many causes such as radiative defects,[17,37] quantum confinement in nanoparticles,[17,38] surface recombination at the nanoparticle surface,[38] and radiative recombination in band tails.[17,39]

The PL signal of samples with an excess of silicon below 4% shows a significant peak observed at 400 nm. This peak can be attributed to defects in the oxide. It has already been observed in samples with small nanocrystals or in defect rich SiO_2.[40] In the present work, for samples with an excess of silicon below 4%, we have very few or may be no excess of silicon leading to a small nanocrystal size (or no nanocrystals at all). This defect may be due to a lack of oxygen as reported by Mikhaylov.[37]

The PL spectra for samples with silicon excess >4% were deconvoluted into two peaks: one peak between 500 and 650 nm and the second one between 700 and 850 nm. According to literature, the second peak is often attributed to the emission of the Si-nanoparticles while the 570 nm PL emission is attributed to defects in the silicon oxide.[41,42] For

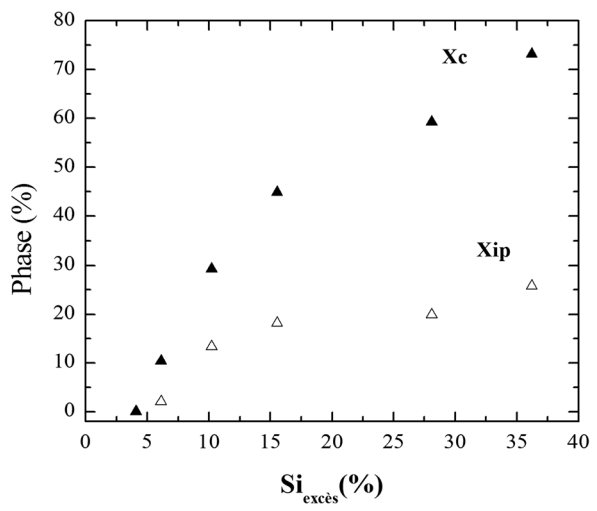

FIG. 8. Crystalline (Xc) and intermediate phase (Xip) volume fraction versus the amount of excess of silicon in the SiON matrix.

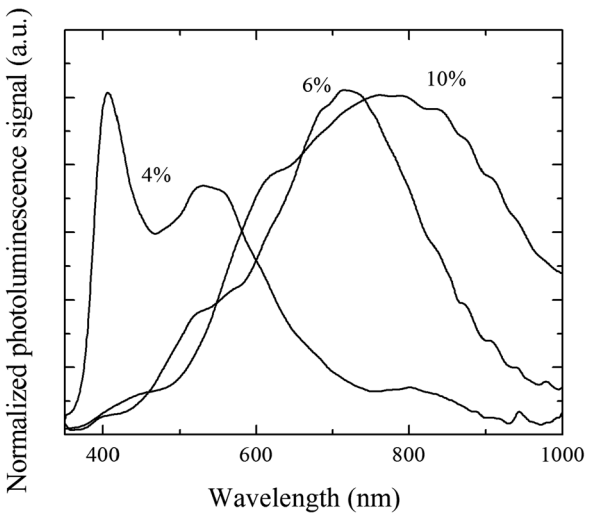

FIG. 9. Photoluminescence spectra recorded for high temperature annealed SRSON layers containing different excess of silicon. The Si excess was determined from RBS analysis. The PL signals are all normalized.

sample with an Si_{excess} = 4%, there is a peak at around 540 nm. This peak could be attributed to the mentioned defects or to very small amorphous silicon nanoparticles. Increasing Si_{excess} up to 10%, the PL peak position is shifted to higher wavelengths. The confinement theory could explain the observed shift of the PL as it was shown above that the size of the nanoparticles increases with the excess of silicon (Figure 6). For samples with a higher excess (>10%), the maximum of PL is shifted to shorter wavelengths. This is in contradiction with the confinement theory since the size is still increasing. One first explication is the shape of the nanoparticles which is not spherical anymore. Indeed there is possibly a larger confinement in one single direction. Another possible explanation is the composition of the matrix surrounding the nanoparticles, which changes with the gas ratio, consequently with Si_{excess}. The effect of the surrounding matrix of the nanoparticles has already been investigated using *ab-initio* calculations considering silicon clusters with different bonding condition with oxygen.[43] In their work, they have shown that the more the Si nanocrystal is oxidized, the smaller is the band gap. In Yang *et al.*,[39] the effect of surface passivation was experimentally studied on silicon rich SiN_x and silicon rich SiO_x layers. In this work, nitrogen and oxygen was found to change the properties of the emission from the Si nanoparticles. For the same diameter, the surrounding matrix change the gap of the PL emission.[3] In our SRSON layers, both nitrogen and oxygen are bonded to the silicon nanoparticle surface. However, the ratio of Si-N and Si-O bonds is strongly varying with the Si excess, which affects seriously the light emission.

Figure 10 plots the optical bandgap as deduced from the PL peak versus the diameter of the silicon nanoparticle. Additional data taken from the literature concerning Si nanoparticles in silicon oxide or silicon nitride matrix are drawn for comparison. Open and full symbols represent, respectively, a silicon oxide or nitride dielectric matrix surrounding the nanoparticle. The surrounding material changes the effective gap of the silicon nanocrystal. This has been explained by *ab initio* calculation.[44] Our results (stars) are in good agreement with literature for samples containing Si nanoparticles with 3 and 4 nm in size diameter while they deviates strongly for samples with larger diameters. For the small Si nanoparticles, the PL can be attributed to the quantum confinement in the silicon nanoparticles. Moreover, the PL emission is almost the same as in an oxide matrix. Different studies showed the high effect of a small amount of oxygen surrounding the silicon nanocrystal by ab initio calculation.[43,45] Only one oxygen bridge is sufficient to decrease the optical bandgap. In fact, if oxygen atoms are double bonded with silicon atoms, the gap is even more reduced.[43] This effective gap reduction seems to saturate when increasing the number of surrounding oxygen.[43,45] This observations mean that a few amount of oxygen present in the dielectric matrix is sufficient to influence significantly the gap of the material.

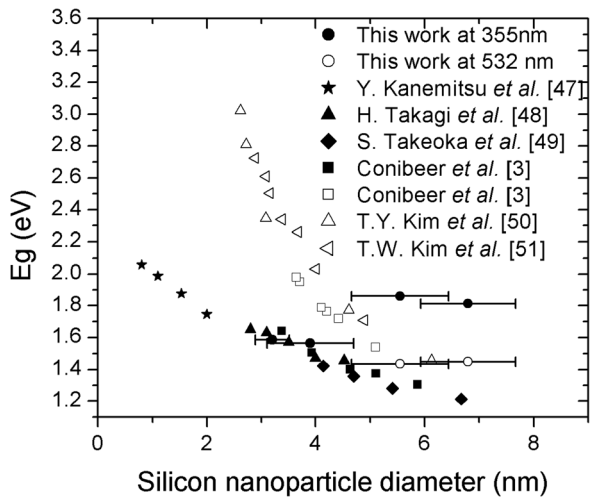

FIG. 10. Variation of bandgap of the material extracted from the PL measurement versus the Si nanoparticle diameter embedded in different matrix. Empty and full symbol represent silicon nanoparticle in, respectively, silicon nitride[3,47–49] and silicon oxide matrix from several authors.[3,50,51]

Figure 10 shows that our bandgap values deviate from the expected behavior for silicon nanoparticles size higher than 5.5 nm (black circles). This suggests that the PL signal is due to another contribution than quantum confinement. The Si objects as defined in the Raman section above might play a role in the luminescence properties of the SRSON layers. The number of these objects increases with the Si excess. It has been shown that this highly disordered silicon is likely to have higher optical gap compared to amorphous silicon.[46] The measured PL signal is possibly due to these Si objects for high excess of silicon (>15%) and can explain the emission at higher energies. In order to hide the PL contribution of these defected silicon and enhance that due to silicon nanoparticles, the SRSON structures with large Si excess (large Si nanoparticles) were excited with a YAG laser emitting at 532 nm (2.33 eV) and the PL recorded. The newly extracted optical bandgaps are also reported in Figure 10 (open circles). These values are in very good agreement with literature data and with the predicted behavior. This result show that the PL response for the large Si nanoparticles obtained with high silicon excess (>15%) is due to emission from Si objects as well as from Si nanocrystals.

IV. CONCLUSIONS

In this work, we have investigated the chemical content, the crystalline properties, and the photoluminescence of deposited SRSON layer, before and after thermal annealing. We have shown that the atomic composition can be easily tuned, thanks to variation of the SiH_4/N_2O gas ratio during plasma deposition. The results show that it is possible to obtain SRSON films with a high nitrogen content and a controllable amount of Si excess. It is assumed that the SRSON separates into two phases during thermal annealing: Si nps and SiON matrix. EFTEM study demonstrated the formation of silicon nanoparticles and their size increases with increasing the silicon excess in the SRSON layer. Moreover, the nanoparticle size can be varied, thanks to the control of the nitrogen content, which is known to hinder the silicon diffusion. On the other hand, Raman measurements revealed that the silicon nanoparticles are characterized by 3 phases: pure crystalline, amorphous, and intermediate phase. The

crystalline fraction of these phases is found to be strongly correlated to the nanoparticle size. Finally, the optical analysis of the SRSON layers through the photoluminescence measurements show that it is also possible to tune the maximum position of the broad and intense PL between 400 and 800 nm by changing the silicon excess in the SRSON matrix.

[1]Z. J. Horváth, Curr. Appl. Phys. **6**, 145 (2006).
[2]L. Pavesi, Mater. Today **8**, 18 (2005).
[3]G. Conibeer, M. Green, E.-C. Cho, D. König, Y.-H. Cho, T. Fangsuwannarak, G. Scardera, E. Pink, Y. Huang, T. Puzzer, S. Huang, D. Song, C. Flynn, S. Park, X. Hao, and D. Mansfield, Thin Solid Films **516**, 6748 (2008).
[4]F. Gourbilleau, C. Dufour, B. Rezgui, and G. Brémond, Mater. Sci. Eng., B **159–160**, 70 (2009).
[5]F. Delachat, M. Carrada, G. Ferblantier, A. Slaoui, C. Bonafos, S. Schamm, and H. Rinnert, Physica E **41**, 994 (2009).
[6]F. Iacona, C. Bongiorno, C. Spinella, S. Boninelli, and F. Priolo, J. Appl. Phys. **95**, 3723 (2004).
[7]A. M. Hartel, D. Hiller, S. Gutsch, P. Löper, S. Estradé, F. Peiró, B. Garrido, and M. Zacharias, Thin Solid Films **520**, 121 (2011).
[8]G.-R. Lin, Y.-H. Pai, C.-T. Lin, and C.-C. Chen, Appl. Phys. Lett. **96**, 263514 (2010).
[9]M. Ribeiro, I. Pereyra, and M. I. Alayo, Thin Solid Films **426**, 200 (2003).
[10]C. M. M. Denisse, K. Z. Troost, J. B. O. Elferink, F. H. P. M. Habraken, W. F. van der Weg, and M. Hendriks, J. Appl. Phys. **60**, 2536 (1986).
[11]S. Perret-Tran-Van, K. Makasheva, B. Despax, C. Bonafos, P. E. Coulon, and V. Paillard, Nanotechnology **21**, 285605 (2010).
[12]P. D. Nguyen, D. M. Kepaptsoglou, Q. M. Ramasse, M. F. Sunding, L. O. Vestland, T. G. Finstad, and A. Olsen, J. Appl. Phys. **112**, 073514 (2012).
[13]G. Mannino, C. Spinella, C. Bongiorno, G. Nicotra, F. Mercorillo, V. Privitera, G. Franzò, A. M. Piro, M. Grimaldi, M. A. Di Stefano, and S. Di Marco, J. Appl. Phys. **107**, 023703 (2010).
[14]F. Ehrhardt, G. Ferblantier, C. Ulhaq-Bouillet, D. Muller, and A. Slaoui, Phys. Status Solidi C **9**, 1878 (2012).
[15]S. Schamm, C. Bonafos, H. Coffin, N. Cherkashin, M. Carrada, G. Ben Assayag, A. Claverie, M. Tencé, and C. Colliex, Ultramicroscopy **108**, 346 (2008).
[16]M. G. Hussein, K. Wörhoff, G. Sengo, and A. Driessen, Thin Solid Films **515**, 3779 (2007).
[17]B. H. Augustine, E. A. Irene, Y. J. He, K. J. Price, L. E. McNeil, K. N. Christensen, and D. M. Maher, J. Appl. Phys. **78**, 4020 (1995).
[18]P. G. Pai, S. S. Chao, Y. Takagi, and G. Lucovsky, J. Vac. Sci. Technol. A **4**, 689 (1986).
[19]D. Criado, I. Pereyra, and M. I. Alayo, Mater. Charact. **50**, 167 (2003).
[20]W. A. Lanford and M. J. Rand, J. Appl. Phys. **49**, 2473 (1978).
[21]F. Delachat, M. Carrada, G. Ferblantier, J.-J. Grob, and A. Slaoui, Nanotechnology **20**, 415608 (2009).
[22]T. Müller, K.-H. Heinig, and W. Möller, Mater. Sci. Eng., B **101**, 49 (2003).
[23]T. Inokuma, Y. Wakayama, T. Muramoto, R. Aoki, Y. Kurata, and S. Hasegawa, J. Appl. Phys. **83**, 2228 (1998).
[24]L. V. Mercaldo, E. M. Esposito, P. D. Veneri, G. Fameli, S. Mirabella, and G. Nicotra, Appl. Phys. Lett. **97**, 153112 (2010).
[25]I. M. Lifshitz and V. V. Slyozov, J. Phys. Chem. Solids **19**, 35 (1961).
[26]C. Wagner, Z. Elektrochem. Ber. Bunsenges. Phys. Chem. **65**, 581 (1961).
[27]M. Roussel, E. Talbot, P. Pareige, and F. Gourbilleau, J. Appl. Phys. **113**, 063519 (2013).
[28]D. Tsoukalas, C. Tsamis, and P. Normand, J. Appl. Phys. **89**, 7809 (2001).
[29]H. Schmidt, U. Geckle, and M. Bruns, Phys. Rev. B **74**, 045203 (2006).
[30]A. Ardell, Acta Metall. **20**, 61 (1972).
[31]Y. Duan, J. F. Kong, and W. Z. Shen, J. Raman Spectrosc. **43**, 756 (2012).
[32]P. G. Han, Z. Y. Ma, Z. Y. Xia, D. Y. Chen, D. Y. Wei, B. Qian, W. Li, J. Xu, X. F. Huang, K. J. Chen, and D. Feng, Nanotechnology **18**, 255703 (2007).
[33]G. Yue, J. D. Lorentzen, J. Lin, D. Han, and Q. Wang, Appl. Phys. Lett. **75**, 492 (1999).
[34]Y. Sui, X. Huang, Z. Ma, W. Li, F. Qiao, K. Chen, and K. Chen, J. Phys.: Condens. Matter **15**, 5793 (2003).
[35]E. Bustarret, M. A. Hachicha, and M. Brunel, Appl. Phys. Lett. **52**, 1675 (1988).
[36]S. Hernández, A. Martínez, P. Pellegrino, Y. Lebour, B. Garrido, E. Jordana, and J. M. Fedeli, J. Appl. Phys. **104**, 044304 (2008).
[37]A. N. Mikhaylov, D. I. Tetelbaum, V. A. Burdov, O. N. Gorshkov, A. I. Belov, D. A. Kambarov, V. A. Belyakov, V. K. Vasiliev, A. I. Kovalev, and D. M. Gaponova, J. Nanosci. Nanotechnol. **8**, 780 (2008).
[38]Y. Kanemitsu, T. Ogawa, K. Shiraishi, and K. Takeda, Phys. Rev. B **48**, 4883 (1993).
[39]M. S. Yang, J. H. Shin, and K. J. Kim, J. Korean Phys. Soc. **48**, 1291 (2006).
[40]W. D. A. M. de Boer, D. Timmerman, K. Dohnalova, I. N. Yassievich, H. Zhang, W. J. Buma, and T. Gregorkiewicz, Nat. Nanotechnol. **5**, 878 (2010).
[41]A. Tewary, R. D. Kekatpure, and M. L. Brongersma, Appl. Phys. Lett. **88**, 093114 (2006).
[42]M. Dovrat, Y. Goshen, J. Jedrzejewski, I. Balberg, and A. Sa'ar, Phys. Rev. B **69**, 155311 (2004).
[43]M. Luppi and S. Ossicini, Phys. Rev. B **71**, 035340 (2005).
[44]D. König, J. Rudd, M. A. Green, and G. Conibeer, Phys. Rev. B **78**, 035339 (2008).
[45]T. J. Pennycook, G. Hadjisavvas, J. C. Idrobo, P. C. Kelires, and S. T. Pantelides, Phys. Rev. B **82**, 125310 (2010).
[46]D. Das and K. Bhattacharya, J. Appl. Phys. **100**, 103701 (2006).
[47]Y. Kanemitsu, J. Lumin. **70**, 333 (1996).
[48]H. Takagi, H. Ogawa, Y. Yamazaki, A. Ishizaki, and T. Nakagiri, Appl. Phys. Lett. **56**, 2379 (1990).
[49]S. Takeoka, M. Fujii, and S. Hayashi, Phys. Rev. B **62**, 16820 (2000).
[50]T.-Y. Kim, N.-M. Park, K.-H. Kim, G. Y. Sung, Y.-W. Ok, T.-Y. Seong, and C.-J. Choi, Appl. Phys. Lett. **85**, 5355 (2004).
[51]T.-W. Kim, C.-H. Cho, B.-H. Kim, and S.-J. Park, Appl. Phys. Lett. **88**, 123102 (2006).